IOP Publishing Journal of Physics: Condensed Matter
J. Phys.: Condens. Matter **32** (2020) 235003 (7pp) https://doi.org/10.1088/1361-648X/ab7579

Enhancement of Rashba spin–orbit coupling by electron confinement at the $LaAlO_3/SrTiO_3$ interface

Mingrui Liu[1,4], Yanpeng Hong[1,2,4], Hongxia Xue[1], Jianchao Meng[1], Weimin Jiang[1], Zhe Zhang[1], Jingzhuo Ling[1], Ruifen Dou[1], Changmin Xiong[1], Lin He[1] and Jiacai Nie[1,3]

[1] Department of Physics, Beijing Normal University, Beijing 100875, People's Republic of China
[2] School of Computational Science and Electronics, Hunan Institute of Engineering, Xiangtan 411104, People's Republic of China

E-mail: jcnie@bnu.edu.cn

Received 23 November 2019, revised 14 January 2020
Accepted for publication 12 February 2020
Published 12 March 2020

Abstract

Electrical transport property is closely related to the dimensionality of carriers' distribution. In this work, we succeed in tuning the carriers' distribution and the Rashba spin–orbit coupling at $LaAlO_3/SrTiO_3$ interface by varying the oxygen pressure (c-P_{O2}) adopted in crystalline $LaAlO_3$ growth. Measurements of the in-plane anisotropic magnetoresistance and the conducting-layer thickness indicate that the carriers' distribution changes from three to two dimensions with c-P_{O2} increasing, i.e. the electron confinement gets stronger. Importantly, by measuring the low-temperature out-of-plane magnetoresistance and analyzing the weak localization/weak anti-localization, we find that the strength of Rashba spin–orbit coupling can be enhanced by electron confinement. The electron confinement is a manifestation of breaking of spatial inversion symmetry. Therefore, our work reveals the intimate relationship between spatial inversion symmetry breaking and Rashba spin–orbit coupling at the $LaAlO_3/SrTiO_3$ interface, and provides a new method to tune the Rashba spin–orbit coupling, which is valuable in the application of oxide-spintronics.

Keywords: $LaAlO_3/SrTiO_3$ interface, electron confinement, spin–orbit coupling, spatial inversion symmetry breaking

(Some figures may appear in colour only in the online journal)

1. Introduction

The quasi-two-dimension electron gas (q-2DEG) formed between $LaAlO_3$ (LAO) and $SrTiO_3$ (STO) has received tremendous attentions in recent years owing to its superior properties such as high mobility [1], superconductivity [2] and ferromagnetism [3]. Remarkably, electrically tunable Rashba spin–orbital coupling (SOC) is discovered at the interface [4], providing unlimited possibilities in applications of spintronics [5, 6] and the exploration of topological phases [7–9].

The Rashba SOC at the LAO/STO interface is interesting because of the hierarchy of d-orbitals [8, 10]; it splits the degenerate d_{yz} and d_{zx} orbitals. The strength of Rashba SOC peaks at the avoided band-crossings [11] and is therefore affected by the level of band filling (e.g. carrier density), which can be tuned by an applied electric field [4]. In addition, the degree of symmetry breaking is another key factor in regulating the Rashba SOC strength, as the Rashba coefficient $\alpha_R = (\hbar/4m^2c^2)\mathrm{d}V(z)/\mathrm{d}z$ depends on the potential gradient $\mathrm{d}V(z)/\mathrm{d}z$ in the z direction due to the spatial inversion asymmetry [11, 12]. At the LAO/STO interface, the inversion asymmetry is related to the electron confinement, i.e. the distribution of carriers across the interface (thickness of

[3] Author to whom any correspondence should be addressed.
[4] Mingrui Liu and Yanpeng Hong made equal contributes to this work.

Table 1. Growth parameters and transport properties.

Samples	*c*-LAO		*a*-LAO			
	T (°C)	*c*-P_{O2} (mbar)	T (°C)	*a*-P_{O2} (mbar)	$n_{s\text{-}2\,K}$ (cm^{-2})	$\mu_{s\text{-}2\,K}$ ($cm^2\,V^{-1}\,s^{-1}$)
A	760	3×10^{-5}	—	—	5.25×10^{13}	1685
B	760	1×10^{-3}	RT	5×10^{-7}	5.95×10^{13}	1212
C	760	5×10^{-3}	RT	3×10^{-7}	5.48×10^{13}	1437
D	760	1×10^{-2}	RT	1×10^{-7}	6.30×10^{13}	121

conducting layer) [4]. Electron transferred from the top layer of LAO to the LAO/STO interface layer due to polar discontinuity (Polar Catastrophe model) [13] is one of the origins of interfacial carriers. However, extra electrons denoted by oxygen vacancies (OVs) created in STO during the growth of crystalline LAO (*c*-LAO) also contribute to the interfacial conductivity [14, 15]. The lower the *c*-P_{O2} during the growth of the *c*-LAO, the deeper the diffusion of OVs into STO. Therefore, the distribution of carriers can be controlled by *c*-P_{O2}. Electron confinement is strengthened as *c*-P_{O2} increases, which has been supported by previous experiments [1, 15–18]. Such properties of LAO/STO interface provide a platform for studying the relationship between symmetry breaking and the Rashba SOC.

In field-effect experiments, an external electric field can alter the dielectric property of STO [18], and subsequently, the carriers' distribution [19, 20]. Nevertheless, as mentioned above, because of the high dielectric constant of STO, the carrier density also changes upon electric gating [4]. This obscures the carriers-distribution dependence of the Rashba SOC in field-effect experiments. In this work, we aim to reveal the intimate relationship between electron confinement and Rashba SOC. The carriers distribution is controlled by adjusting *c*-P_{O2} in the growth of *c*-LAO. To eliminate the effects of band filling, samples are prepared with similar electron densities by coating an amorphous LAO (*a*-LAO) layer [21], as detailed in section 3.1. In section 3.2, the relation of the electron confinement and *c*-P_{O2} is demonstrated qualitatively and quantitatively by measurements of the in-plane anisotropic magnetoresistance (AMR) and orbital effect. In addition, the Rashba SOC is enhanced upon the strengthening of the electron confinement, demonstrated in section 3.3, by examining the out-of-plane magnetoresistance of the samples and subsequent weak localization (WL)/anti-localization (WAL) analyses. Our work provides a new method to control the Rashba SOC at the LAO/STO interface, which may pave the way for further research.

2. Experiments

Atomically flat single-crystal STO (0 0 1, $[TiO_2]^0$-terminated) substrates were obtained by chemical etching and subsequent annealing [22, 23]. To control the distribution of electrons across the interface, 3 nm *c*-LAO were grown by pulsed laser deposition (PLD) (KrF, $\lambda = 248$ nm) on treated STO substrate from a single-crystal LAO target under a wide range of *c*-P_{O2}. The high-*c*-P_{O2}-grown ($\geqslant 10^{-3}$ mbar) *c*-LAO/STO samples were insulating. In order to achieve an insulator–metal transition and control their carrier density, *a*-LAO (5 nm) was prepared on the top of *c*-LAO/STO samples at room temperature (RT) under various oxygen pressure (*a*-P_{O2}) by PLD. The physical mechanism will be elaborated in section 3.1. The growth parameters of the selected samples with similar sheet carrier density are listed in table 1. The laser frequency is 1 Hz and the energy density of the laser spot is 1 J cm^{-2}.

The surface morphology of *c*-LAO/STO was examined by atomic force microscopy (AFM). It could be seen from figure 1 that up to *c*-$P_{O2} = 1 \times 10^{-2}$ mbar, the surfaces of *c*-LAO films are all atomically flat and show terraces that originate from the treated STO substrates (not shown); however, the surface roughness is slightly larger in the samples grown under higher *c*-P_{O2}. Electric and magneto-transport properties were measured using a Physical Property Measurement System (PPMS, Quantum Design).

3. Results

3.1. Insulator–metal transition in high-c-P_{O2}-grown samples

A typical *c*-LAO/STO grown under low *c*-P_{O2} (3×10^{-5} mbar) is metallic from 300 to 2 K (see figure 2, sample A). However, a *c*-LAO/STO grown under high *c*-P_{O2} ($\geqslant 1 \times 10^{-3}$ mbar, sample B, C, and D) is insulating which is consistent with previous experimental results [24–27]. Chen *et al* [21] succeeded in realizing insulator–metal transition in insulating *c*-LAO/STO by capping *a*-LAO. They pointed that the *a*-LAO layer works as an electron reservoir (possibly originates from OVs) which transfers electrons to the interface. Meanwhile, it was pointed out in several theoretical works that transfer of electrons donated by OVs at the surface of *c*-LAO to the interface is possible because of the built-in field in *c*-LAO [28, 29].

Hence, in this work, *a*-LAO layers are grown on the insulating *c*-LAO/STO samples in reducing environment (*a*-P_{O2} is lower than 1×10^{-6} mbar) to introduce OVs at the surface of *c*-LAO [21, 30]. As expected, insulator–metal transition is observed among these samples, as shown in figure 2 (sample B, C, and D). Furthermore, the sheet carrier density n_s in these *a*-LAO/*c*-LAO/STO samples can be tuned by *a*-P_{O2}, which is intuitive in that *a*-P_{O2} affects the amount of OVs generated at the surface of *c*-LAO, and thus the amount of electron transferred. On the contrary, the *c*-LAO/STO (1 1 0) grown under high *c*-P_{O2} is still insulating after capping *a*-LAO, which proves that *a*-LAO does not affect the OVs in the side of STO. In other words, the effect of covering *a*-LAO on the

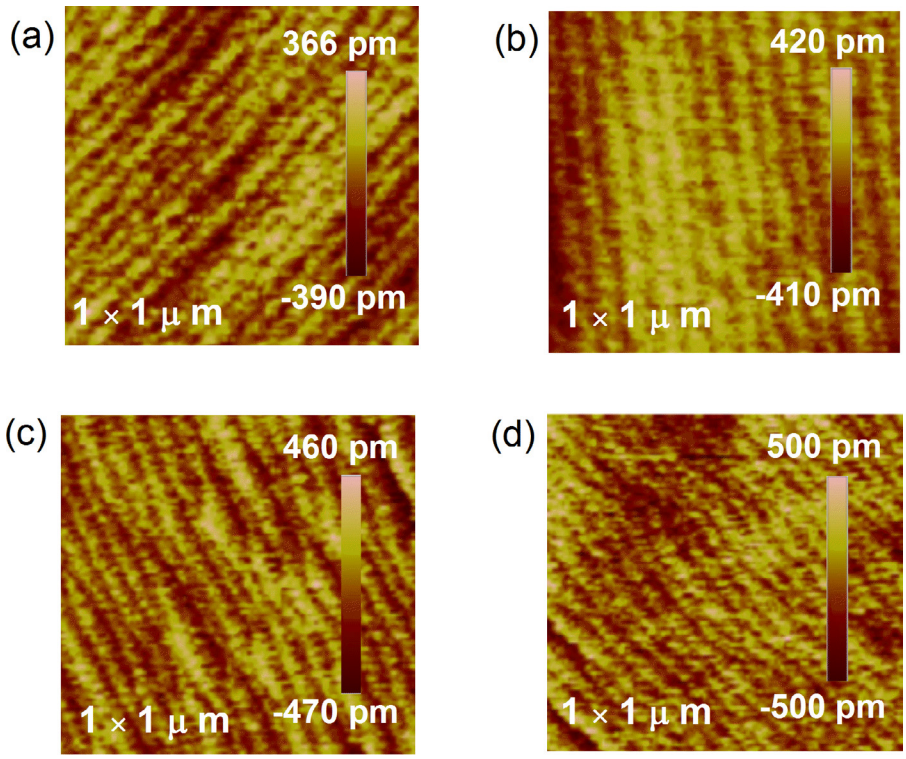

Figure 1. AFM images of samples (a) A (c-$P_{O2} = 3 \times 10^{-5}$ mbar), (b) B (c-$P_{O2} = 1 \times 10^{-3}$ mbar), (c) C (c-$P_{O2} = 5 \times 10^{-3}$ mbar), and (d) D (c-$P_{O2} = 1 \times 10^{-2}$ mbar).

thickness of the conducting layer is negligible, which is also supported by the measurements of the electron confinement in section 3.2.

In order to eliminate the effects of the carrier density on the Rashba SOC, various-c-P_{O2}-grown (corresponding to various thickness of conducting layer) samples with the same level of sheet carrier density n_s (controlled by the capping a-LAO layers with various a-P_{O2}) are selected in this study. The inset in figure 2 shows the transverse resistance R_{xy} measurements at 2 K. The sheet carrier density n_s and carrier mobility μ_s were evaluated and are presented in table 1. At 2 K, the mobility decreases with the growth of c-P_{O2}. The mobility of sample D is much lower (only 121 $cm^2\,V^{-1}\,s^{-1}$), which is considered to be due to the enhanced WL caused by a strong electron confinement, as will be discussed in the Discussion section.

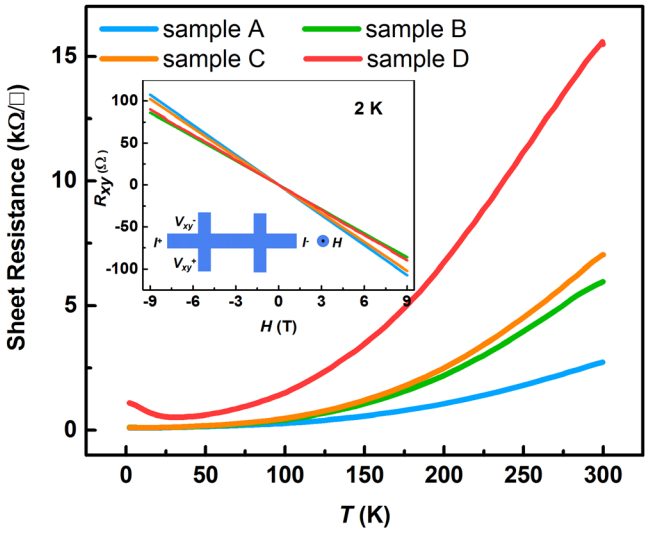

Figure 2. Temperature-dependent sheet resistance of sample A, B, C, and D from 300 to 2 K. Inset: transverse resistance R_{xy} measurements of various samples at 2 K.

3.2. Electron confinement

To further confirm the strengthening of the electron confinement by increasing the c-P_{O2}, the in-plane AMR is first compared among samples grown under various c-P_{O2}. Here, AMR is defined as

$$\mathrm{AMR} = \frac{R(H,\theta) - R(H,0)}{R(H,0)} \times 100\%,$$

where θ is the angle between the direction of the magnetic field and the current (figure 3(a)). The in-plane resistance is $R\,(H)_\perp$ [$R\,(H)_\parallel$] when the magnetic field is perpendicular (parallel) to the current.

The in-plane AMR for sample A, B, C and D are shown in figure 3(b). Measurements are performed at 2 K with a magnetic field of 9 T. For sample A and B, the oscillation period of $R(\theta)$ is twofold and $R\,(H)_\perp > R\,(H)_\parallel$. However, the tendency is reversed with $R(H)_\perp < \mathrm{R}(H)_\parallel$ in sample D. The in-plane AMR of sample C is similar to that of sample D, showing $R\,(H)_\perp < R\,(H)_\parallel$ but with small additional peaks being exhibited at $\theta = 90°$ and 270°. Flekser *et al* [16] and Annadi *et al* [17] had already established the relationship between the dimension of electron distribution and the feature of in-plane AMR: when the electron distribution is three-dimensional (3D), the orbital effect lengthens the transport

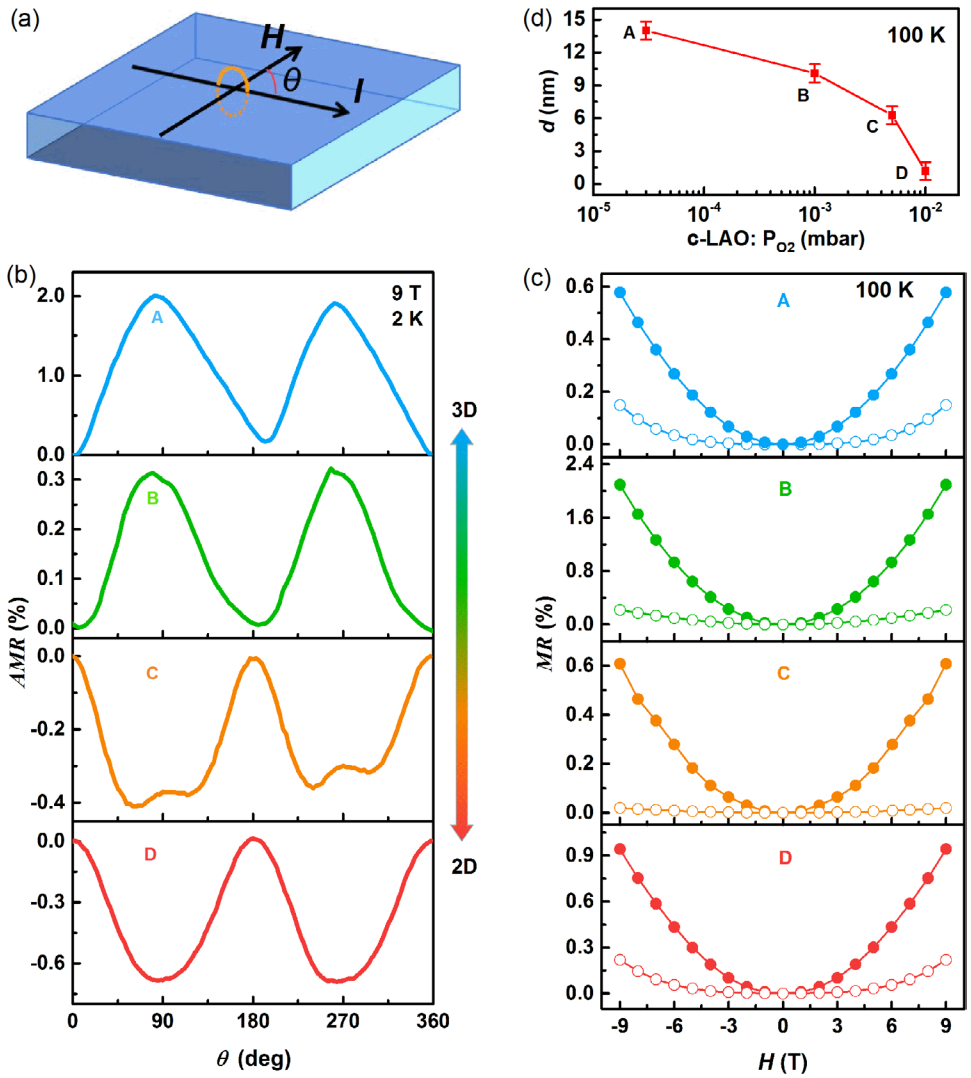

Figure 3. (a) Schematic of AMR measurement, where the direction of magnetic field H is parallel to the interface and the angle θ between the magnetic field direction H and current I is varied. When $H \perp I$, the electrons are scattered (orange circle) due to Lorentz forces perpendicular to the plane, which lengthens the transport path of electron (i.e. orbital effect). In the contrast, when $H \parallel I$, electrons are not affected by Lorentz forces during transport. (b) In-plane AMR in a 9 T field at 2 K of sample A, B, C and D. (c) Out-of-plane (solid circle) and in-plane (open circle) $MR_{\perp}$ of sample A, B, C and D at 100 K. (d) Relationship between the thickness of the conducting layer and the c-P_{O2} of c-LAO at 100 K.

path of electron, leading to $R\ (H)_{\perp} > R\ (H)_{\parallel}$ (elaborated in the caption of figure 3(a)); however, when the electron distribution is close to two-dimensional (2D), the orbital effect is suppressed because of the reduced thickness of conducting layer. Therefore, it can be inferred clearly from figure 3(b) that there is a crossover of electron distribution from 3D to 2D as we increase the c-P_{O2} in the growth of c-LAO.

Quantitatively, the thickness of interfacial conducting layer could be estimated by comparing the in-plane and out-of-plane orbital effect [19]:

$$\frac{\mathrm{MR}_{\perp,\text{in-plane}}}{\mathrm{MR}_{\perp,\text{out-of-plane}}} = \left(\frac{d}{l}\right)^2,$$

where d is the thickness of conducting layer, $l = \frac{h}{e^2 k_F R_S}$ and $\mathrm{MR} = \frac{R(B)-R(0)}{R(0)} \times 100\%$. Based on this method, our group had previously succeeded in determining the temperature dependence of the conducting layer thickness of LAO/STO [20]. It should be noted that at low temperatures, quantum effects such as Rashba SOC or magnetism will appear at this interface and obscure the orbital effect, therefore we employ this method by measuring MR at 100 K instead. In figure 3(c), the $MR_{\perp}$s are all positive at 100 K, indicating the dominance of the orbital effect and validating the feasibility of this method. By calculating the ratio of in-plane $MR_{\perp}$ and out-of-plane $MR_{\perp}$ at 9 T, the conducting layer thickness is measured to decreased monotonously from approximately 14 nm in sample A to 1.18 nm in sample D, as shown in figure 3(d). This result is consistent with the observations in the in-plane AMR measurements, and confirms quantitatively our conclusion that an increase in c-P_{O2} in the growth of c-LAO strengthens the electron confinement. Although the conducting layer thickness is

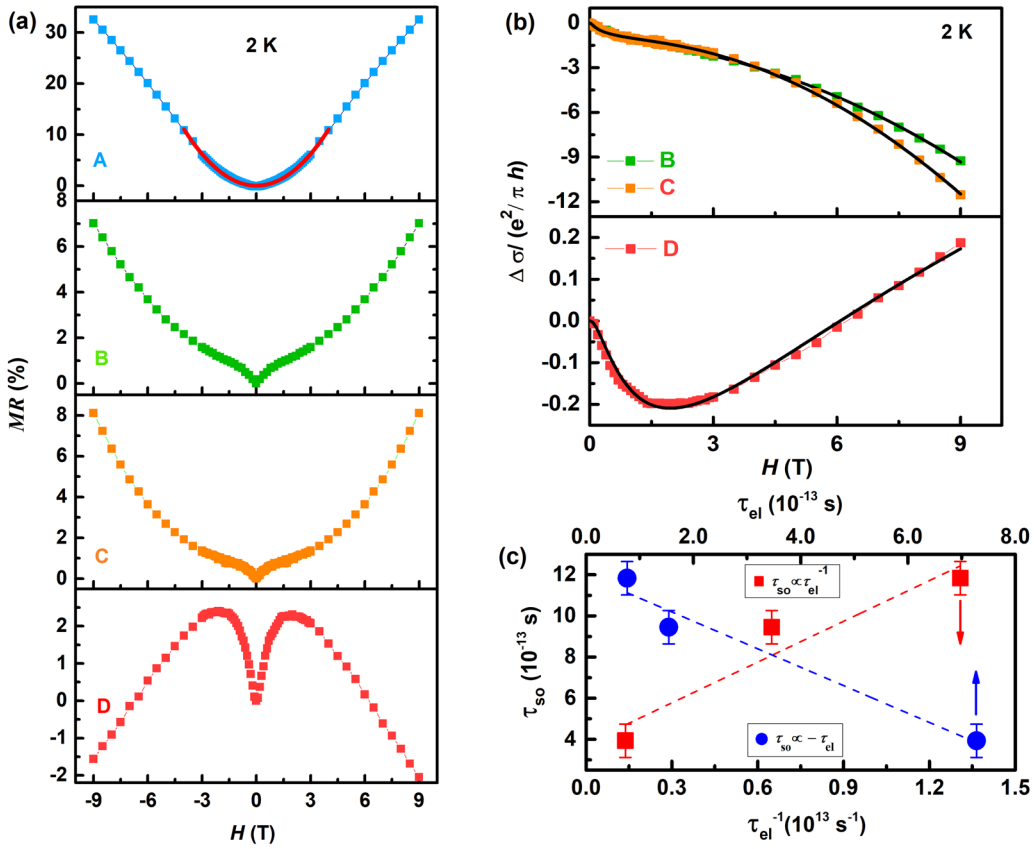

Figure 4. (a) Out-of-plane $MR_{\perp}$ of sample A, B, C and D at 2 K. (b) MF fittings of the out-of-plane $MR_{\perp}$ of sample B, C and D at 2 K. (c) Relation of τ_{so} and τ_{el}, showing $\tau_{so} \propto \tau_{el}^{-1}$. The dotted line is linear fitting.

obtained by measuring the orbital effect at 100 K, according to our previous work [20], this should be true at lower temperature as well.

3.3. Enhancement of Rashba SOC

The out-of-plane $MR_{\perp}$ is measured at 2 K to investigate the effect of the electron confinement on the strength of Rashba SOC (figure 4(a)). Essential differences can be seen in figure 4(a): for sample A with the thickest conducting layer, the out-of-plane $MR_{\perp}$ is positive and is a square function of the magnetic field (solid line of sample A in figure 4(a)), indicating the dominance of orbital effect and negligible WL or WAL [19]; as the thickness of the conducting layer decreases, cusps appear at low fields in out-of-plane $MR_{\perp}$ of sample B and C (figure 4(a)), indicating the appearance of WAL [4]; for sample D, with the thinnest conducting layer, WAL exists at low field as well and, in addition, the out-of-plane $MR_{\perp}$ turns negative at high field.

The WL stems from constructive interference of two time-reversed electron-diffusion paths and enhances the backscattering of diffusive conduction electrons, manifesting itself as positive correction to the resistance. A perpendicular magnetic field would alter the phase of electron path and destroy the constructive interference, resulting in negative MR [31]. If SOC exists, the two time-reversed electron-diffusion paths will interfere each other destructively, leading to negative correction to the resistance (WAL). In this case, if a perpendicular magnetic field is applied, the alignment of spins will change so that the destructive interference is no longer satisfied, resulting in positive MR [31].

The appearances of WAL in sample B, C, and D indicate firmly that the strength of the Rashba SOC is enhanced compared to sample A. To illustrate this more quantitatively, we fit the out-of-plane $MR_{\perp}$s by the Maekawa–Fukuyama (MF) formula [32]:

$$\frac{\Delta\sigma}{\sigma_0} = -\psi\left(\frac{1}{2}+\frac{B_{el}}{B}\right)+\frac{3}{2}\psi\left(\frac{1}{2}+\frac{B_{in}+B_{so}}{B}\right)-\frac{1}{2}\psi\left(\frac{1}{2}+\frac{B_{in}}{B}\right) - \ln\left(\frac{B_{in}+B_{so}}{B_{el}}\right)-\frac{1}{2}\ln\left(\frac{B_{in}+B_{so}}{B_{in}}\right)-A_k\frac{\sigma(0)}{\sigma_0}B^2.$$

Here, $\sigma_0 = e^2/\pi h$ is the quantum of conductance with e the elementary charge and h the Plank constant. ψ is the digamma function. B_{el}, B_{in} and B_{so} are the effective fields related to elastic relaxation time τ_{el}, inelastic relaxation time τ_{in} and spin–orbit relaxation time τ_{so}, respectively. We add an approximate B^2 term with A_k the Kohler coefficient to account for the orbital magnetoconductance due to Lorentz force; however A_k is zero of sample D, further indicating that the orbital effect is suppressed because of electron confinement. The fitting reproduces the results of out-of-plane $MR_{\perp}$ well, as indicated by solid lines in figure 4(b). Although the original WL/WAL theory considered only a single conduction band, it has been demonstrated that the single-band WL/WAL theory is also valid for multiband systems [33–35] and has been successfully applied to LAO/STO system [36, 37]. Note

Table 2. Results of MF fitting.

Samples	B_{so} (T)	B_{in} (T)	L_{el} (nm)	L_{in} (nm)	L_{so} (nm)	E_{so}(meV)
A	0	0	—	—	—	—
B	0.25	0.017	59.93	98.02	25.68	8.53
C	0.44	0.02	16.58	90.80	19.36	10.9
D	0.62	0.16	8.79	32.10	16.31	13.8

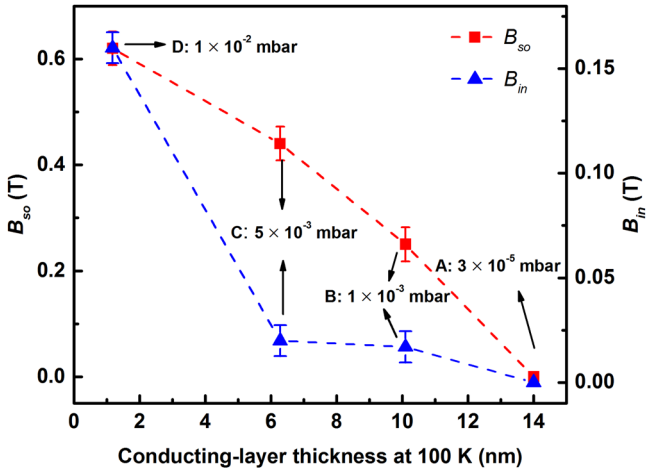

Figure 5. Conducting layer dependence of the strength of Rashba SOC and WL. Dashed lines serves as guides for eyes. The sample name and c-P_{O2} used in the growth c-LAO are indicated. Note that the conducting layer dependence is measured at 100 K.

that the out-of-plane $MR_\perp$ of sample A cannot be fitted by the MF formula, demonstrating again that it is dominated by the orbital effect and WL/WAL is negligible.

The main results of fitting are listed in table 2. B_{so}, B_{in} can be directly extracted from the fitting, B_{el} is estimated from Hall mobility $B_{el} = e/2\mu^2\hbar^2k^2$. The phase coherent length L_{in} and the spin relaxation length L_{so} can be calculated as $L_{in,so} = \sqrt{\hbar/4eB_{in,so}}$, where is the reduced Planck constant. The mean free path L_{el} is estimated in the free-electron model: $L_{el} = 3D/v_F$, with $D = v_F^2\tau_{el}/2$ the diffusion constant and $v_F = \hbar k_F/m^*$ the Fermi velocity. $k_F = \sqrt{2\pi n_s}$ is the Fermi vector in two dimensions. We set $m^* = 3m_e$ [38], where m_e is the free electron mass. $\tau_{el} = \sqrt{m^{*2}/(2e\hbar k^2 B_{el})}$ and $\tau_{so} = m^{*2}/(2e\hbar k^2\tau_{el}B_{so})$ [37]. In the WL/WAL framework, the coherent backscattering takes place when $L_{el} < L_{in}$, which is satisfied by our fitting results of each samples. It can be seen from figure 4(c) that the spin relaxation satisfies D'yakonov–Perel' (DP) mechanism, i.e. $\tau_{so} \propto \tau_{el}^{-1}$ [39]. On the contrary, plotting τ_{so} versus τ_{el} will result in a negative slope (figure 4(c)), excluding the Elliot–Yafet spin-relaxation mechanism [40]. In the DP mechanism, the spin splitting energy due to Rashba SOC can be calculated as $E_{so} = \hbar/\sqrt{\tau_{so}\tau_{el}}$ [36, 41].

The B_{so} as a function of conducting layer thickness is shown in figure 5. B_{so} increases from 0.25 to 0.62 T as the thickness of conducting layer decreases. Meanwhile, L_{so} decreases from 25.68 to 16.31 nm and E_{so} increases from 8.53 to 13.8 meV (table 2). Note that the carrier densities in these samples are similar, which suggests that the enhancement of Rashba SOC is due to the enhancement of electron confinement when the c-P_{O2} in the growth c-LAO increases from sample A to D. As c-P_{O2} increases, the electron distribution approaches 2D. Consequently, the electrons are more strongly confined to the interface and suffer from the spatial inversion asymmetry, which is a crucial factor in Rashba SOC [11, 12].

4. Discussion

The out-of-plane $MR_\perp$ of sample D turns negative at high fields (figure 4(a)). This is atypical because at LAO/STO, a negative out-of-plane $MR_\perp$ usually exists in low-carrier-density samples (usually lower than 10^{13} cm^{-2}, [4]). However, as shown in table 2 and figure 5, the inelastic field B_{in} of sample D is approximately eight times larger than sample A, which means that the negative out-of-plane $MR_\perp$ is attributed to the enhancement of WL in sample D. The strengthening of WL by electron confinement is a natural consequence because the WL is stronger in 2D than in 3D [42]. This is also supported by the significantly reduced mobility of sample D (table 1). Meanwhile, the result of WL/WAL analysis is consistent with that of in-plane AMR: the disappearance of peaks at $\theta = 90°$ and 270° in figure 3(a) corresponds to the zero Kohler coefficient A_k, indicating the vanishing orbital effect in sample D with more confined electrons.

Other possible origin of the observed negative out-of-plane $MR_\perp$ is magnetism, which is often observed at LAO/STO [3, 43] or LAO/Fe-doped STO [44, 45]. As the electron distribution approaches 2D, more and more electrons tend to reside at the interface layer and the portion of partially filled d-orbitals increases. Because that the d-electron possesses a magnetic moment, magnetism (Kondo effect [43] or ferromagnetism [3, 46–48]) may also play a role.

5. Conclusion

In summary, LAO/STO heterostructures were grown in a wide range of c-P_{O2}, in order to investigate the effect of electron confinement on the Rashba SOC. By covering a-LAO, we realized an insulator–metal transition in the high-c-P_{O2}-grown samples and regulated their sheet carrier densities to similar levels. Evaluating the strength of electron confinement in these samples by measuring the in-plane AMR and orbital effect, a crossover of the electron distribution from 3D to 2D was observed as c-P_{O2} increases from 3×10^{-5} to 1×10^{-2} mbar. In the study of the out-of-plane $MR_\perp$, the Rashba SOC is enhanced with decreasing the thickness of conducting layer, despite the similarity of carrier densities of the selected samples. We proposed that it is the strengthened electron confinement that aggravates the spatial inversion asymmetry, to which the electrons are subjected in transport,

that leads to the enhancement of Rashba SOC. Our work demonstrates the possibility in tuning the Rashba SOC at the LAO/STO heterostructure by varying the dimensionality of electron distribution, which is meaningful in the application of oxide-spintronics.

Acknowledgments

This work was supported by the National Natural Science Foundation of China (Grants No. 11674031, No. 11474022, No. 11474024, No. 11422430, and No. 11374035) and the National Basic Research Program of China (Grants No. 2014CB920903 and No.2013CB921701).

ORCID iDs

Mingrui Liu https://orcid.org/0000-0001-7275-4790
Ruifen Dou https://orcid.org/0000-0003-2831-045X
Lin He https://orcid.org/0000-0001-5251-1687

References

[1] Ohtomo A and Hwang H Y 2004 *Nature* **427** 423–6
[2] Reyren N *et al* 2007 *Science* **317** 1196–9
[3] Brinkman A *et al* 2007 *Nat. Mater.* **6** 493–6
[4] Caviglia A D, Gabay M, Gariglio S, Reyren N, Cancellieri C and Triscone J M 2010 *Phys. Rev. Lett.* **104** 126803
[5] Žutić I, Fabian J and Sarma S D 2004 *Rev. Mod. Phys.* **76** 323–410
[6] Lesne E *et al* 2016 *Nat. Mater.* **15** 1261–6
[7] Hasan M Z and Kane C L 2010 *Rev. Mod. Phys.* **82** 3045–67
[8] Gariglio S, Caviglia A D, Triscone J and Gabay M 2019 *Rep. Prog. Phys.* **82** 012501
[9] Scheurer M S and Schmalian J 2015 *Nat. Commun.* **6** 6005
[10] Santander-Syro A F *et al* 2011 *Nature* **469** 189–93
[11] Zhong Z, Toth A and Held K 2013 *Phys. Rev.* B **87** 161102
[12] Khalsa G, Lee B and Macdonald A H 2013 *Phys. Rev.* B **88** 041302
[13] Nakagawa N, Hwang H Y and Muller D A 2006 *Nat. Mater.* **5** 204–9
[14] Chen Y, Pryds N, Kleibeuker J E, Koster G, Sun J, Stamate E, Shen B, Rijnders G and Linderoth S 2011 *Nano Lett.* **11** 3774–8
[15] Basletic M *et al* 2008 *Nat. Mater.* **7** 621–5
[16] Flekser E, Ben Shalom M, Kim M, Bell C, Hikita Y, Hwang H Y and Dagan Y 2012 *Phys. Rev.* B **86** 121104
[17] Annadi A *et al* 2013 *Phys. Rev.* B **87** 201102
[18] Hemberger J, Lunkenheimer P, Viana R, Bohmer R and Loidl A 1995 *Phys. Rev.* B **52** 13159–62
[19] Ben Shalom M, Tai C-W, Lereah Y, Sachs M, Levy E, Rakhmilevitch D, Palevski A and Dagan Y 2009 *Phys. Rev.* B **80** 140403
[20] Xue H *et al* 2017 *Phys. Rev.* B **96** 235310
[21] Chen Z *et al* 2018 *Adv. Mater. Interfaces* **5** 1801216
[22] Koster G, Kropman B L, Rijnders G, Blank D and Rogalla H 1998 *Appl. Phys. Lett.* **73** 2920–2
[23] Han Y-L *et al* 2014 *Appl. Phys. Lett.* **105** 192603
[24] Kalabukhov A, Gunnarsson R, Borjesson J, Olsson E, Claeson T and Winkler D 2007 *Phys. Rev.* B **75** 121404
[25] Mannhart J, Blank D H A, Hwang H Y, Millis A J and Triscone J M 2008 *MRS Bull.* **33** 1027–34
[26] Siemons W, Koster G, Yamamoto H, Harrison W A, Lucovsky G, Geballe T H, Blank D H A and Beasley M R 2007 *Phys. Rev. Lett.* **98** 196802
[27] Herranz G *et al* 2007 *Phys. Rev. Lett.* **98** 216803
[28] Zhou J, Asmara T C, Yang M, Sawatzky G A, Feng Y P and Rusydi A 2015 *Phys. Rev.* B **92** 125423
[29] Bristowe N C, Littlewood P B and Artacho E 2011 *Phys. Rev.* B **83** 205405
[30] Li C *et al* 2018 *Sci. Rep.* **8** 404
[31] Bergmann G 1984 *Phys. Rep.* **107** 1–58
[32] Maekawa S and Fukuyama H 1981 *J. Phys. Soc. Japan* **50** 2516–24
[33] Rainer D and Bergmann G 1985 *Phys. Rev.* B **32** 3522–9
[34] Buchstab E I, Butenko A V, Fogel N Y, Cherkasova V G and Rosenbaum R L 1994 *Phys. Rev.* B **50** 10063–8
[35] Stornaiuolo D, Gariglio S, Fete A, Gabay M, Li D, Massarotti D and Triscone J M 2014 *Phys. Rev.* B **90** 235426
[36] Liang H, Cheng L, Wei L, Luo Z, Yu G, Zeng C and Zhang Z 2015 *Phys. Rev.* B **92** 075309
[37] Huijben M, Hassink G W J, Stehno M P, Liao Z L, Rijnders G, Brinkman A and Koster G 2017 *Phys. Rev.* B **96** 075310
[38] Mattheiss L F 1972 *Phys. Rev.* B **6** 4740–53
[39] Dyakonov M I and Perel V I 1972 *Sov. Phys. Solid State* **13** 3023–6
[40] Boross P, Dora B, Kiss A and Simon F 2013 *Sci. Rep.* **3** 3233
[41] Chiu S-P, Yamanouchi M, Oyamada T, Ohta H and Lin J 2017 *Phys. Rev.* B **96** 085143
[42] Datta S 1995 *Electronic Transport in Mesoscopic Systems* (Cambridge: Cambridge University Press)
[43] Lee M, Williams J R, Zhang S, Frisbie C D and Goldhaber-Gordon D 2011 *Phys. Rev. Lett.* **107** 256601
[44] Zhang H *et al* 2018 *Phys. Rev.* B **97** 155150
[45] Xue H *et al* 2018 *Phys. Rev.* B **98** 085305
[46] Dikin D A, Mehta M, Bark C W, Folkman C M, Eom C B and Chandrasekhar V 2011 *Phys. Rev. Lett.* **107** 056802
[47] Bert J A, Kalisky B, Bell C, Kim M, Hikita Y, Hwang H Y and Moler K A 2011 *Nat. Phys.* **7** 767–71
[48] Li L, Richter C, Mannhart J and Ashoori R C 2011 *Nat. Phys.* **7** 762–6